Chapter 2
Quantum Tomography

2.1 Introduction

In practice, the experimenter always has to verify that the three components of a quantum experiment—state preparation, transformation, and measurement—are close to what the theorist wants them to be. The first step towards this is classical characterization of the devices (e.g. testing a waveplate with a laser against a reference), which especially in optics can go a long way to estimating the performance of the device in a quantum experiment [1]. On the other hand, if the goal is to reconstruct which state (or channel, or measurement) the experiment actually implemented, quantum tomography is the gold-standard. Just like tomography in medical imaging, the aim is to reconstruct the unknown state from a large number of snapshots taken at various angles, see Fig. 2.1. In contrast to the classical case, where all measurements are performed on the same patient, a quantum measurement necessarily disturbs the state of the system. As a consequence, it is not possible to reconstruct the exact quantum state of a single particle, and quantum tomography always reconstructs the (average) quantum state of an ensemble of identically prepared particles.

A set of different snapshots that contains enough information to fully determine any quantum state is called an *informationally-complete* set of measurements. For a d-dimensional system, with $d^2 - 1$ free parameters, the minimal number of measurements in such a set is d^2. One measurement for each parameter and one additional measurement to normalize the experimental frequencies into probabilities. In a very similar fashion, tomography of a measurement uses an informationally complete set of preparations. Up to an additional parameter that can be interpreted as a bias, the measurement also corresponds to a vector on the Bloch sphere, see also Sect. 1.3.

M. Ringbauer, *Exploring Quantum Foundations with Single Photons*, Springer Theses,
DOI 10.1007/978-3-319-64988-7_2

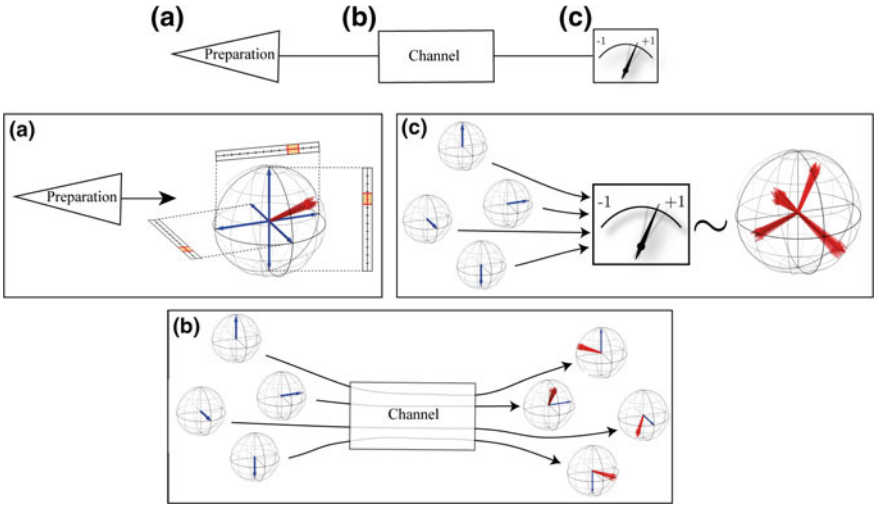

Fig. 2.1 Quantum tomography. Every quantum experiment can be broken up into state preparation, evolution, and measurement. The aim of quantum tomography is to characterize the experimental implementation of these three steps. **a** Quantum state tomography aims to characterize the quantum state produced in the state-preparation step. This is achieved by subjecting this state to a set of well-calibrated measurements. **b** Quantum process tomography aims to reconstruct a description of the evolution of arbitrary states through the quantum channel. This is achieved by reconstructing the output states (using quantum state tomography) for a set of well-characterized input states. **c** Quantum Measurement Tomography aims to reconstruct a description of the measurement that is implemented by a given measurement device. By probing the measurement device with a set of well-characterized input states, it is possible to reconstruct the measurement operators from the observed statistics

2.2 Quantum State Tomography

Consider, for example, a single qubit, whose state $\rho = (\mathbb{1} + \vec{n} \cdot \vec{\sigma})/2$ is completely described by the $d^2 - 1 = 3$ real valued parameters that are the components of the Bloch-vector (n_X, n_Y, n_Z), see Fig. 2.1. The simplest procedure to find the quantum state is thus by performing measurements along the axes of the Bloch sphere in order to determine the components of the Bloch vector individually. This is an example of a set of *mutually unbiased bases*, which are sets of orthonormal bases, such that the modulus squared of the inner product between elements of different bases is a constant $1/d$, see Fig. 2.2a. In other words, any state from one of these bases has equal probability for all outcomes when measured in any of the other bases in the set. This latter property is particularly interesting for applications such as quantum cryptography. Although it is unclear whether such sets exist in general, they are known to exist for the most relevant cases of Hilbert spaces with prime-power dimension [2]. This includes multi-qubit spaces, which makes these sets the most widely used measurement for multi-qubit quantum tomography.

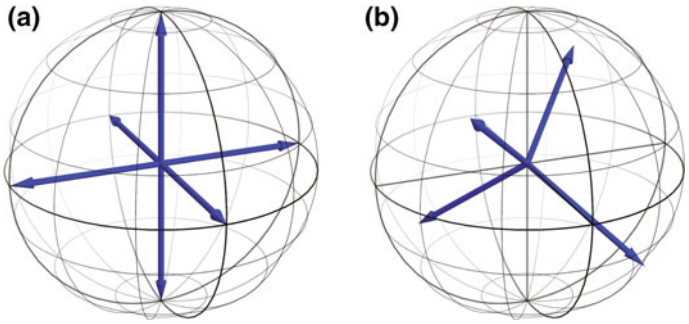

Fig. 2.2 The two most relevant choices of tomographically complete measurements for a single qubit. **a** The standard tomography set consists of the mutually unbiased bases corresponding to the Pauli operators, i.e. the axes of the Bloch-sphere. **b** The minimal set of measurements in the form of a symmetric informationally POVM forms a tetrahedron in the Bloch-sphere. In this case all projectors are sub-normalized to $1/2$ to satisfy the normalization of probabilities required for a POVM

In practice, these measurements are often the easiest and most precise. However, they are *over-complete* in the sense that they use more than the d^2 required measurements. As in the classical case, more measurements typically means more reliable results, but at the same time the number of measurements required to characterize a multi-qubit system scales exponentially with the number of qubits. One way to reduce the number of measurements is to only measure one outcome for each axes except one, and assume that the total number of events is the same along every axis. This, however, is a rather asymmetric arrangement of measurements. A more important class of minimal sets of tomography measurements are so-called *symmetric informationally-complete*(SIC) POVMs [3]. They consist of d^2 subnormalized projectors, which have a fixed inner product and are thus arranged symmetrically in the respective Hilbert space. Such measurements are conjectured to exist in every dimension, but their existence has only been shown numerically for dimensions up to 67. In the case of a single qubit the outcomes of the SIC POVM correspond to the vertices of a regular tetrahedron, see Fig. 2.2.

2.2.1 Linear Inversion Tomography

In practice, the simplest algorithm for quantum tomography is linear inversion. In the following, the notation of Ref. [4] is used and the interested reader is referred to Ref. [4] for a more in-depth discussion. Consider the problem of state-tomography of a d-dimensional system using a set of informationally complete (potentially over-complete) measurement operators $\{E_i\}_{i=1}^{K}$, with $K \geq d^2$. Using vectorized notation, the expected probabilities for the various measurement outcomes are then given by $P_i = \mathrm{Tr}[E_i \rho] = \langle\langle E_i | \rho \rangle\rangle$. One can then define a vector $|P\rangle$ of observed probabilities, a matrix S of vectorized measurement operators, and a matrix W of weights [4]

$$
\begin{aligned}
|P\rangle &= \sum_{i=1}^{K} P_i |i\rangle \\
S &= \sum_{i=1}^{K} |i\rangle \langle\langle E_i | \\
W &= \sum_{i=1}^{K} w_i |i\rangle\langle i| \ .
\end{aligned}
\tag{2.1}
$$

Here, $|i\rangle$ denotes the unit vector with a single 1 at index i, and $w_i \geq 0$ are weights which specify the relative importance of the various measurements. The matrix S contains the vectorized measurement operators, such that in the ideal case $S\,|\rho\rangle\!\rangle = |P\rangle$. The linear inversion problem is finding a $\hat{\rho}_{\text{LIN}}$ that satisfies the equation $S\,|\rho\rangle\!\rangle = |P\rangle$. This estimator is given by

$$
\hat{\rho}_{\text{LIN}} = (S^\dagger S)^{-1} S^\dagger |P\rangle \ . \tag{2.2}
$$

In the case of a tomographically complete or over-complete set of measurements, the matrix $(S^\dagger S)$ is indeed invertible [4], otherwise the Moore-Penrose pseudo-inverse can be used. The linear inversion estimator is a special case of a weighted least-squares fit [4]

$$
\hat{\rho} = \text{argmin}_\rho \, \| W S\,|\rho\rangle\!\rangle - W|P\rangle \|_2 \ , \tag{2.3}
$$

where $\| \cdot \|_2$ is the Euclidean vector norm. This has the analytic solution

$$
\begin{aligned}
\big|\hat{\rho}\big\rangle\!\big\rangle &= (S^\dagger W^\dagger W S)^{-1} S^\dagger W^\dagger W |P\rangle \\
&= \sum_i w_i^2 P_i \left(\sum_k w_k^2 |E_k\rangle\!\rangle\langle\langle E_k| \right)^{-1} |\,E_i\rangle\!\rangle \ ,
\end{aligned}
\tag{2.4}
$$

which, in the case of uniform weights $w_i = 1$, reduces to Eq. (2.3).

This simple technique, however, does not cope very well with imperfect experimental data. As a result of experimental noise, the obtained estimator $\hat{\rho}_{\text{LIN}}$ is typically not a valid (i.e. positive semi-definite, Hermitian, trace-one) density matrix [5, 6]. The problem is that the procedure does not know how a physical density matrix looks like and simply finds a matrix that works.

2.2.2 *Maximum Likelihood Estimation*

The main problem of linear inversion, that the result is typically unphysical, can be overcome by only searching the space of valid density matrices for a solution. This

solution can in general not be expected to reproduce the observed data perfectly, but it is the physical state that is most likely to have produced the observed data.

To formalize this, note that the probability for jointly observing a set of counts $\{n_1, \ldots, n_K\}$ from measurements $\{E_i, \ldots, E_K\}$, given that the measured quantum state is ρ, is simply the product of the individual probabilities. Turning this around, the same product describes the *likelihood* L that the measured state was ρ, given that the set of counts $\{n_1, \ldots, n_K\}$ was observed

$$L(\rho|\{n_i\}) = P(\{n_i\}|\rho) = \prod_{i=1}^{K} P(n_i|\rho) \ , \tag{2.5}$$

The goal of *maximum likelihood estimation* [7, 8] is to find the quantum state $\hat{\rho}_{\text{MLE}}$ that maximizes the likelihood function, or equivalently minimizes the negative log-likelihood function (which turns out to be computationally more stable). To make the optimization computationally tractable it is typically assumed that the probability of observing n_i counts from the measurement E_i is well approximated by a normal distribution centred around the estimator $\text{Tr}[E_i\rho]$

$$P(n_i|\rho) \propto \exp\left[-\frac{(n_i - N_i \,\text{Tr}[E_i\rho])^2}{2\sigma_i^2}\right] \ . \tag{2.6}$$

Here, N_i denotes the total number of counts in the basis that contains the measurement E_i. This takes into account that, due to loss or other factors, it cannot be assumed that the total number of counts is the same in every basis. For computational reasons it is also convenient to approximate the estimator-variance σ_i^2, which a priori depends on ρ, by the constant variance of the observed counts n_i. When conditioned on a fixed N_i the (unconditionally Poisson-distributed) counts n_i follow a binomial distribution with variance $\sigma_i^2 \sim N_i\, p_i(1 - p_i)$. Hence, the approximation of this distribution by a normal distribution is only valid for large N_i, and when $p_i \neq 0, 1$. Under these conditions maximum likelihood estimation solves the optimization problem [4]:

$$\begin{aligned} \hat{\rho}_{\text{MLE}} &= \arg\min_{\rho}[-\log L(\rho|\{n_i\})] \\ &= \arg\min_{\rho} \sum_{i=1}^{K} \frac{(n_i - N_i \,\text{Tr}[E_i\rho])^2}{N_i\, p_i(1 - p_i)} \ . \end{aligned} \tag{2.7}$$

As shown in Ref. [4] this can be recast as a constrained least-squares optimization

$$\begin{aligned} &\text{minimize} \quad \|WS\,|\,\rho\rangle\rangle - W|p\rangle\|_2 \\ &\text{subject to:} \quad \rho \geq 0, \quad \text{Tr}[\rho] = 1 \ , \end{aligned} \tag{2.8}$$

where the weights are chosen such that

$$w_i = \frac{N_i}{\sigma_i} = \sqrt{\frac{N_i}{p_i(1-p_i)}}\,, \tag{2.9}$$

The linear inversion method of Eq. (2.3) is a special case where the constraints of Eq. (2.8) are dropped and uniform weights $w_i = 1$ are used. Since the objective function $\|\cdot\|_2$ in Eq. (2.8) is convex and the constrains are semidefinite, the problem can be solved numerical as a *semidefinite program*. See Ref. [4] for more details.

2.2.3 Zero Probabilities

If any of the tomography measurements happen to return zero counts, the estimator may assign a probability of zero to it. However, no finite dataset can do justice to a probability of zero[1] [9] since it cannot exclude the possibility that this event is just very unlikely. Moreover, the normal approximation in Eq. (2.9) breaks down and it is not possible to assign any non-zero error to the estimate either [9]. In the case of binary-outcome measurements, a simple way to avoid zero probabilities is to add a small amount of noise [4, 10] to the observed counts, defining the observed probabilities

$$f_i = \frac{n_i + \beta}{N_i + 2\beta}\,, \tag{2.10}$$

where the factor of 2 in the denominator equals the number of measurements used to normalize the experimental frequencies (i.e. 2 for a two-outcome measurement). The *hedging* parameter β can be chosen freely, but a value of $\beta \sim \frac{1}{2}$ works well in most cases, except almost pure states, where lower values work better [4, 11]. This approach works well to avoid zero-probabilities in the data, but it cannot guarantee that the reconstructed state doesn't *predict* zero probabilities. In particular in situations with low statistics and an unlucky experimenter, it can happen that, even after adding β, the linear inversion solution still lies outside the Bloch-sphere. The maximum likelihood estimator in this case would lie on the surface of the sphere and thus predict probability zero for orthogonal measurements. This can be avoided using *hedged maximum likelihood estimation* [11] where the standard likelihood function of Eq. (2.5) is replaced by product $L(\rho|\{n_i\})\det(\rho)^\beta$. The optimization problem is then

$$\begin{aligned} &\text{minimize} \quad \frac{1}{2}\|WS\,|\,\rho\rangle\rangle - W|p\rangle\|_2^2 - \beta\log\det(\rho) \\ &\text{subject to:} \quad \rho \geq 0, \quad \mathrm{Tr}[\rho] = 1\,. \end{aligned}$$

[1] As discussed in Ref. [9], maximum likelihood estimation is a frequentist tool, which works in the asymptotic limit of infinite sample size, but "applying a frequentist method to relatively small amounts of data is inherently disaster-prone".

This effectively pushes the estimator away from the boundary, but does not change it significantly if beta is chosen as above. In the case of measurements in only a single basis, this actually recovers Eq. (2.10) exactly [11].

2.2.4 Error Bars for Quantum Tomography

Both linear inversion and maximum likelihood estimation produce point estimates $\hat{\rho}$. Since such estimates can never hope to match the true ρ exactly (except in the asymptotic limit), they are only physically meaningful if they have some uncertainty bounds. In the special case of polarization qubits, error estimation for tomography has been discussed in Ref. [8]. More generally, standard approaches typically use the variance of the point estimator to define ellipsoidal confidence regions. These regions, however, might include unphysical states, even if the point estimator is physical. This can in general be avoided by constructing the regions via bootstrapping methods [12] that perform many iterations of the tomography on either resampled experimental data or experimental data with simulated statistical noise. This method is used in large parts of the material presented later in this thesis.

However, also the latter method quantifies the variance of the point estimator, which, in maximum likelihood methods, is in general biased by the positivity constraint (except in the asymptotic limit) [5, 13]. Indeed, maximum likelihood estimators typically *underestimate* the fidelity with the true state [5, 6], and the uncertainty regions of such a biased estimator are in general suboptimal [13]. In contrast, linear inversion estimators are unbiased but unphysical in a large number of cases and produce larger mean squared errors, which makes them of limited use in practice [6].

A reliable error region for maximum likelihood estimation should contain the true state with high probability and contain no unphysical states. One suggestion that satisfies these requirements are the *likelihood ratio confidence regions* $R_\alpha(D)$ introduced in Ref. [13].

$$R_\alpha(D) = \{\rho \mid \lambda(\rho) < \lambda_\alpha\} , \tag{2.11}$$

where $\lambda(\rho)$ is the log-likelihood ratio $\lambda(\rho) = -2\log[\mathcal{L}(\subset)/\max_{\rho'} \mathcal{L}(\rho')]$ and λ_α is a threshold level, such that region $R_\alpha(D)$ contains the true ρ with probability at least α. The region $R_\alpha(D)$ is a convex region and is proven to be a near-optimal region estimator [13]. Practically, however, these regions are difficult to work with since they generally do not have an explicit description and can have quite arbitrary shapes.

2.2.5 Quantum Process Tomography

Besides quantum state tomography, one of the most important motivations for quantum tomography is to reconstruct the quantum process $\mathcal{E}$ implemented by the experi-

ment. Although the experimenter typically has some prior knowledge what he or she intended to build, this can in principle also be done in a completely black-box fashion. Since a quantum channel maps density matrices to other density matrices one has to reconstruct the output state for each of an informationally complete set of inputs. The linearity of quantum mechanics implies that this is sufficient to know how an arbitrary input state evolves. Intuitively, knowing how the axes of the Bloch-sphere are transformed is enough to know how every point of the sphere is transformed. Exploiting the Choi-Jamiolkowski isomorphism the reconstruction of a quantum process $\mathcal{E}$ acting on a d-dimensional system can be mapped to state-tomography of the d^2-dimensional Choi matrix $\Lambda_{\mathcal{E}}$. Using Eq. (1.23) the probability p_{ij} for observing the measurement outcome E_j given that the state ρ_i was subject to the process is

$$p_{ij} = \mathrm{Tr}[E_j^\dagger \, \mathrm{Tr}_1[(\rho^T \otimes \mathbb{1})\Lambda_{\mathcal{E}}] = \mathrm{Tr}[(\rho^T \otimes E_j^\dagger)\Lambda_{\mathcal{E}}] = \langle\!\langle \rho^* \otimes E_j | \Lambda_{\mathcal{E}} \rangle\!\rangle \ .$$

Note that ρ^* is now interpreted as a "measurement" on the Choi matrix. With this identification one can then use the same tools as for quantum state tomography to formulate quantum process tomography as a constrained optimization problem [4]

$$\begin{aligned} &\text{minimize} \quad \| W S \, | \Lambda_{\mathcal{E}} \rangle\!\rangle - W | p \rangle \|_2 \\ &\text{subject to:} \quad \Lambda_{\mathcal{E}} \geq 0, \quad \mathrm{Tr}[\Lambda_{\mathcal{E}}] = d \ , \end{aligned} \tag{2.12}$$

with $S = \sum_{i,j=1}^{K} |i\rangle \langle\!\langle \rho_i^* \otimes E_j \, |$ and straight-forward generalizations of $|p\rangle$, and W from Eq. (2.1). In contrast to state tomography, the Choi matrix is normalized such that $\mathrm{Tr}[\Lambda_{\mathcal{E}}] = d$ rather than 1.

Practicality
Since the number of measurements required for process tomography of an n-qubit process scales as 2^{4n}, it quickly becomes impractical. Hence, it would be desirable to use (partially) classical methods to quickly assess the performance of a quantum process without the constraints of process tomography. In a *dual-rail* picture, where the two levels of the qubit correspond to two distinct paths, any n-qubit quantum channel can be described by a $2n$ linear optical network of beam-splitters and phase-shifters. The process is then conveniently represented by a $2n \times 2n$ *transfer matrix*, which describes how every input mode is mapped to every output mode. Characterizing the matrix amounts to measuring the amplitudes and phases of every entry, which can be done with a coherent state exciting one or at most two input ports [1].

2.2.6 Caveats and Generalizations

One of the challenges of tomography is to avoid circularity. State tomography relies on well-characterized measurements, but to verify the measurements, well-characterized states are needed. A priori there is no ultimate reference to compare

against. As a consequence, the results of quantum tomography can be quite confounded by errors in state preparation and/or measurement. Consider, for example, a single qubit prepared by a polarizer and a set of waveplates. The state tomography might return a purity of 0.9 for this state, which might of course be a result of the system getting entangled with the environment. However, since linear optics is blessed (or cursed) with quantum systems that do not interact much with anything, a more likely explanation is that the tomographic measurements were simply not performing as expected (e.g. unbalanced loss).

Randomized Benchmarking and Gate-Set Tomography

In practice, state preparation uses a fixed element, such as a polarizer or ground-state cooling, followed by a rotation, that is, a quantum channel. Similarly, measurements are implemented using a rotation, followed by a fixed projection, typically in the computational basis. These elements can often be characterized classically to estimate their performance in the experiment. In linear optics, for example, polarizers based on birefringent crystals reliably split an incoming beam into two orthogonal polarizations with a practical extinction ratio of at least $1 : 10^4$. Importantly, these elements are fixed throughout the experiment and are typically very repeatable, which suggests that the crucial aspect is the characterization of quantum processes and the dynamical elements in the experiment.

Randomized benchmarking [14, 15] addresses this challenge using sequences of quantum gates which are chosen at random, such that they ideally add up to the identity. These sequences are applied to a fixed input state and the output is measured using a fixed two-outcome measurement. Since all sequences are decompositions of the identity, all output states should be the same. However, due to error accumulation the fidelity decreases with the length of the sequence, and the slope of fidelity vs. sequence-length gives an estimate of the average error per gate.

Gate-set tomography [16] goes a step further and aims to provide a complete characterization of the experiment without requiring prior knowledge or perfect references. The experiment is treated as a black-box that can implement a discrete set of quantum gates (buttons on the box). In addition, the box is capable of repeatably preparing an input state and performing a two-outcome measurement in the end. In contrast to other techniques, including randomized benchmarking, there are only very mild assumptions on preparation and measurement, such as repeatability of preparation and measurement, but it is not necessary to know the input state or the measurement that was performed. The collected data for different gate-series is used to reconstruct the gate-set, input state and measurement, up to a gauge freedom. In contrast to randomized benchmarking, which averages over coherent errors such as over-rotations, gate-set tomography is sensitive to these errors and provides a better picture of what is actually happening [17]. Gate-set tomography is also robust against local maxima in the likelihood function [16].

Although these methods are in principle independent of the physical implementation, they are particularly useful in architectures like ion traps, where quantum systems are (mostly) stationary and transformations are induced by lasers, which enables long sequences of many randomly chosen operations. Linear optics, on the

other hand, is a bit special in this regard since gates are realized by actual physical elements rather than laser pulses, and the length of the gate-sequence can thus not be changed as dynamically.

2.3 Taming Non-completely-Positive Maps with Superchannels

This section is based on the publication "Characterizing Quantum Dynamics with Initial System-Environment Correlations" [18].

So far, quantum tomography was concerned with isolated quantum systems and processes. In real-world experiments, however, quantum systems are inevitably coupled to an environment, which typically acts as a source of noise, but may also be harnessed as a resource—for example in initializing quantum states that may be otherwise unobtainable [19–26]. In either case understanding the joint behaviour of system and environment is essential. Quantum mechanics postulates that the joint system-environment (SE) state evolves unitarily, which need not be true for the system alone. The theory of open quantum systems nevertheless allows for an operationally complete description of the reduced dynamics of the system, in the case that the initial system-environment state is uncorrelated [27], see Fig. 2.3a. This central assumption is often, however, at best an approximation [28, 29].

In practice, system and environment may be correlated even before the initial state of the system is prepared. Although the state preparation erases all pre-existing correlations, it might leave the environment in a different state depending on which state of the system was prepared. When these different environment states couple to the evolution again at a later stage, the implemented process is not just non-unitary, but also non-CP [4, 18, 28], see Fig. 2.3. Consider, for example, the extreme case of a maximally entangled initial system-environment state: $\frac{1}{\sqrt{2}}(|00\rangle + |11\rangle)_{\mathrm{SE}}$. A projective preparation of the system into $|0\rangle$ or $|1\rangle$ leaves the environment in orthogonal states. Hence, if the subsequent system evolution is not perfectly isolated, it is coupled to different environment states leading to drastically different reduced dynamics of the system conditional on the used preparation procedure [30]. Standard characterization techniques may in this case return a description of the reduced system dynamics that appears unphysical [28, 31–34]. On the other hand, when complete-positivity is enforced, such as in maximum likelihood quantum process tomography, the reconstructed map does not reliably describe the system dynamics.

While the environment is typically inaccessible to the experimenter, recent results suggest that at least partial information about the initial joint system-environment state can be extracted from measurements of the system alone. Initial correlations can be witnessed through the distinguishability [35–38] and purity [39] of quantum states, which has also been explored experimentally [40–42]. A more operationally complete characterisation can be obtained by using a *quantum superchannel* $\mathcal{M}$, which explicitly uses the system's preparation procedure, rather than the prepared

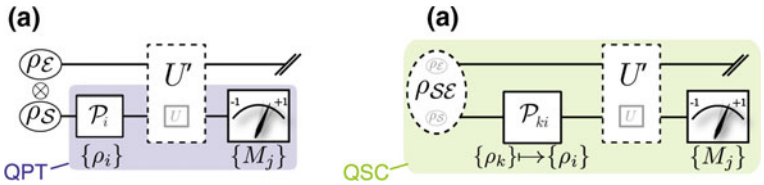

Fig. 2.3 Quantum tomography with an environment. **a** Quantum process tomography (QPT) is designed for a scenario where an isolated quantum system is prepared in the initial state ρ_S and undergoes a joint unitary evolution U with the environment. Process tomography can reconstruct the reduced dynamics of an informationally complete set of states $\{\rho_{\text{in}}^i\}$ and a tomographically complete set of measurements $\{M_j\}_{j=1}^d$ for each input. **b** The situation depicted in (a) is at best an approximation of the real state of affairs. In any realistic scenario the system is initially correlated with the environment, even before the state preparation procedure $\mathcal{P}$. Furthermore, the evolution $\mathcal{U}$ is in general also affected by the environment. The quantum superchannel (QSC) takes all these effects into account and treats the experiment as a whole. It can be reconstructed from an informationally complete set of preparation procedures and measurements

state, as an input [34], see Fig. 2.3b. This superchannel approach captures not just the system evolution, but also the dynamical influence of the environment, even in the presence of initial system-environment correlations. Remarkably, it can be experimentally reconstructed using only measurements on the system, and contains quantitative information about the initial correlations and the influence of the environment.

2.3.1 Constructing the Superchannel $\mathcal{M}$

Consider the situation in Fig. 2.3b, where a system with Hilbert space $\mathcal{X}_1$, and an environment with Hilbert space $\mathcal{Y}_1$ are initially in the joint state $\rho_{\text{SE}} \in L(\mathcal{X}_1 \otimes \mathcal{Y}_1)$. In the following $L(\mathcal{H})$ denotes the set of linear operators on the space $\mathcal{H}$, and $T(\mathcal{H}_1, \mathcal{H}_2)$ denotes the set of linear transformation from the space $\mathcal{H}_1$ to the space $\mathcal{H}_2$. The joint state ρ_{SE} is then subject to a preparation procedure $\mathcal{P} = (\mathcal{P}_{\text{S}} \otimes \mathcal{I}_{\text{E}}) \in T(\mathcal{X}_1 \otimes \mathcal{Y}_1, \mathcal{X}_2, \otimes \mathcal{Y}_2)$, where $\mathcal{Y}_2 = \mathcal{Y}_1$ (due to the identity operation), $\mathcal{I}_{\text{E}}$ is the identity channel on the environment, and $\mathcal{P}_{\text{S}} \in T(\mathcal{X}_1, \mathcal{X}_2)$ acts only on the system to prepare it in a desired input state. This is followed by coupled evolution of the joint system-environment state, described by a CPTP map $\mathcal{U} \in T(\mathcal{X}_2 \otimes \mathcal{Y}_2, \mathcal{X}_3 \otimes \mathcal{Y}_3)$, see Fig. 2.3b. The output is then given by

$$\begin{aligned}\rho'_{\text{S}} &= \text{Tr}_{\mathcal{Y}_3}\left[\mathcal{U}(\mathcal{P}_{\text{S}}(\rho_{\text{SE}}))\right] \\ &= \text{Tr}_{\mathcal{X}_2,\mathcal{Y}_2,\mathcal{Y}_3}\left[\left(\mathcal{P}(\rho_{\text{SE}})^T \otimes \mathbb{1}_{\text{SE}}\right)\Lambda_{\mathcal{U}}\right] \\ &= \text{Tr}_{\mathcal{X}_2,\mathcal{Y}_2,\mathcal{Y}_3}\left[\left(\text{Tr}_{\mathcal{X}_1,\mathcal{Y}_1}\left[\left(\rho_{\text{SE}}^T \otimes \mathbb{1}_{\text{SE}}\right)\Lambda_{\mathcal{P}}\right]^T \otimes \mathbb{1}_{\text{SE}}\right)\Lambda_{\mathcal{U}}\right]. \end{aligned} \tag{2.13}$$

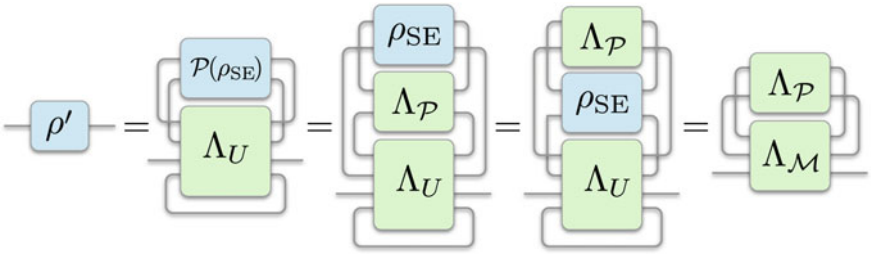

Fig. 2.4 Graphical derivation of the superchannel $\mathcal{M}$ for describing the reduced dynamics of a system initially correlated with the environment. Note that $\Lambda_{\mathcal{U}}$ and $\Lambda_{\mathcal{P}}$ each have 4 subsystem indices, which correspond to S-input, E-input, S-output and E-output, respectively, and different colors are used to distinguish Choi matrices (*green*) from density matrices (*blue*). The expression in Eq. (2.13) corresponds to the third term. Since all tensor wires are contracted the position of $\rho_{\rm SE}$ and $\Lambda_{\mathcal{P}}$ can be exchanged and the preparation procedure can be treated as the effective input state. The Choi matrix $\Lambda_{\mathcal{M}}$ of the superchannel is then defined as the contraction of $\rho_{\rm SE}$ and $\Lambda_{\mathcal{U}}$, equivalently to the index contraction given in Eq. (2.14).

Fig. 2.4 illustrates the construction of the superchannel $\mathcal{M}$ to describe the evolution of Eq. (2.13), and visualizes how it is related to the Choi matrix of the joint evolution. The equivalent definition of the superchannel Choi matrix $\Lambda_{\mathcal{M}}$ in terms of tensor indices is derived in the supplement of Ref. [18], and given by

$$(\Lambda_{\mathcal{M}})_{i_1 i_2 i_3 | j_1 j_2 j_3} = \sum_{n,m,l} (\rho_{\rm SE})_{i_2 n | j_2 m} (\Lambda_{\mathcal{U}})_{i_1 n i_3 l | j_1 m j_3 l} \ , \tag{2.14}$$

By construction, $\Lambda_{\mathcal{M}} \geq 0$ if $\mathcal{U}$ is CP. However, the same does not hold true for TP. If $\mathcal{U}$ is TP, then

$$\mathrm{Tr}_{\mathcal{X}_3}[\Lambda_{\mathcal{M}}] = \mathrm{Tr}_{\mathcal{Y}_1}[\rho_{\rm SE}] \otimes \mathbb{1}_{\mathcal{X}_2} \ . \tag{2.15}$$

Hence $\mathcal{M}$ is TP if and only if $\mathrm{Tr}_{\mathcal{Y}_1}[\rho_{\rm SE}] = \mathbb{1}_{\mathcal{X}_1}$, which is the case only for a maximally entangled initial state or if the system is initially in a completely mixed state. In all other cases, different preparation procedures lead to different overall count rates and the superchannel is not trace preserving. For a TP map $\mathcal{U}$, the Choi matrix for $\mathcal{M}$ has normalization

$$\mathrm{Tr}[\Lambda_{\mathcal{M}}] = \mathrm{Tr}[\mathcal{U}(\mathbb{1}_{\mathcal{X}_1} \otimes \mathrm{Tr}_{\mathcal{X}_1}[\rho_{\rm SE}])] = d_{\mathcal{X}_1} \ . \tag{2.16}$$

The quantum superchannel $\mathcal{M} \in T(\mathcal{X}_1 \otimes \mathcal{X}_2, \mathcal{X}_3)$ thus takes the system-preparation procedure $\Lambda_{\mathcal{P}_{\rm s}} \in L(\mathcal{X}_1 \otimes \mathcal{X}_2)$ as an input and produces an output quantum state $\rho' \in L(\mathcal{X}_3)$ given by

$$\begin{aligned} \rho' &= \mathcal{M}(\Lambda_{\mathcal{P}_{\rm s}}) \\ &= \mathrm{Tr}_{\mathcal{X}_1,\mathcal{X}_2}[(\Lambda_{\mathcal{P}_{\rm s}} \otimes \mathbb{1}_{\mathcal{X}_3}) \Lambda_{\mathcal{U}}] \ . \end{aligned}$$

2.3.2 Superchannel Tomography

The crucial property of the superchannel Choi matrix $\Lambda_{\mathcal{M}}$ is that *all* environment indices are contracted and it can thus be tomographically reconstructed from measurements on the system alone. Since the superchannel takes a preparation procedure as an input, this requires an informationally complete set of *preparation procedures*, rather than just a set of prepared states, as well as an informationally complete set of measurements for each output state. A projective preparation procedure $\mathcal{P}_{ij} \in T(\mathcal{X}_1, \mathcal{X}_2)$, consists of an initial projection (or postselection) onto the state ρ_i followed by a rotation to the state ρ_j. The corresponding Choi matrix is thus given by

$$\Lambda_{\mathcal{P}_{ij}} = \rho_i^* \otimes \rho_j \ ,$$

where * denotes complex conjugation. The probability of observing a click when preparing a state using $\Lambda_{\mathcal{P}_{ij}}$ and then measuring the system by projecting onto a state ρ_k is given by

$$\begin{aligned} p_{ijk} &= \mathrm{Tr}\left[\rho_k^\dagger \, \mathrm{Tr}_{12}[(\rho_i^\dagger \otimes \rho_j^T \otimes \mathbb{1}_{\mathcal{X}_3})\Lambda_{\mathcal{M}}]\right] \\ &= \mathrm{Tr}\left[(\rho_i^\dagger \otimes \rho_j^T \otimes \rho_k^\dagger)\Lambda_{\mathcal{M}}\right] \\ &= \langle\!\langle \rho_i \otimes \rho_j^* \otimes \rho_k | \Lambda_{\mathcal{M}} \rangle\!\rangle = \langle\!\langle \Pi_{ijk} | \Lambda_{\mathcal{M}} \rangle\!\rangle \ , \end{aligned}$$

where $\Pi_{ijk} \equiv \rho_i \otimes \rho_j^* \otimes \rho_k$. For an informationally complete set of states $\{\rho_i\}_{i=1}^K$, with $K \geq d^2$, one can generalize the vector $|p\rangle$, and matrices S and W introduced in Sect. 2.2.1 to

$$\begin{aligned} f_{ijk} &= \frac{n_{ijk} + \beta}{N_{ijk} + 4\beta} \\ |p\rangle &= \sum_{i,j,k=1}^{K} f_{ijk} |i, j, k\rangle \\ S &= \sum_{i,j,k=1}^{K} |i, j, k\rangle \left\langle\!\left\langle \Pi_{ijk} \right| \right. \\ W &= \sum_{i,j,k=1}^{K} w_{ijk} |i, j, k\rangle\langle i, j, k| \ , \end{aligned} \tag{2.17}$$

where f_{ijk} are the hedged experimental frequencies to avoid issues associated with zero probabilities, see Sect. 2.2.3. The total number of events N_{ijk}, which is unknown a priori, is defined by totalling the observed counts for measurement configurations that sum to the identity. Note that the second index of Π_{ijk} corresponds to the rotated state for the initial projective preparation procedure, and only the first and third indices correspond to true measurements. The experimental frequencies are thus normalized to $d^2 = 4$ counts, which leads to the factor of 4 in the definition of the

hedged frequencies. For the choice of weights w_{ijk} a normal approximation for the distribution of the observed probabilities p_{ijk} is assumed, so that

$$w_{ijk} = \sqrt{\frac{N_{ijk}}{p_{ijk}(1-p_{ijk})}} \, .$$

As with quantum state- and process- tomography, one can use maximum likelihood estimation, see Sect. 2.2.2, to reconstruct the Choi matrix of the superchannel $\Lambda_{\mathcal{M}}$, by solving the constrained optimization problem

$$\begin{aligned} &\text{minimize} \quad \|WS\,|\,\Lambda_{\mathcal{E}}\rangle\rangle - W|p\rangle\|_2 \\ &\text{subject to:} \quad \Lambda_{\mathcal{E}} \geq 0, \quad \text{Tr}[\Lambda_{\mathcal{E}}] = d \, . \end{aligned} \tag{2.18}$$

Recall that enforcing complete positivity in maximum likelihood tomography is an effective way of combating statistical noise, which might lead to apparent non-CP dynamics. However, in the presence of initial system-environment correlations the reduced evolution of the system would be genuinely non-CP, which can thus not be correctly reconstructed using maximum likelihood quantum process tomography. In contrast, the superchannel $\mathcal{M}$ fully takes the effect of state preparation into account and is therefore always a completely positive map. As a consequence, the additional constraint of maximum likelihood estimation is justified for overcoming statistical noise, even in the presence of initial correlations.

2.3.3 *Superchannels in the Wild*

To demonstrate the use of the superchannel in practice, consider the evolution of a single photonic qubit, coupled to, and correlated with an environment, see Fig. 2.5. The experimenter aims to implement the target system evolution described by the unitary operator U_{S}, chosen as either a Pauli-Z gate ($U_{\text{S}} = Z$), a Hadamard-gate ($U_{\text{S}} = H = R_{\text{Y}} Z R_{\text{Y}}^{\dagger}$), or a rotation ($U_{\text{S}} = Z R_{\text{Y}}$), where R_{Y} denotes a $\pi/4$-rotation around σ_y. Due to coupling to the environment the reduced dynamics of the system will in general deviate from that described by U_{S}. This can be simulated by replacing the Z operations in the above decomposition of U_{S} by controlled Z (CZ) operations, switched on and off conditional on the state of the environment, which is modelled as another photonic qubit.[2] In the case of Z and H the environment might thus cause a failure of the system unitary (i.e. the identity operation is implemented), while in the case $U_{\text{S}} = Z R_{\text{Y}}$ it can introduce a phase error.

The initial system-environment state was generated via spontaneous parametric downconversion in the form

[2] This is sufficient to describe a large range of joint system-environment dynamics including common error channels, and to illustrate the technique [40, 43], although a slightly larger environment would be required in the most general case [44, 45].

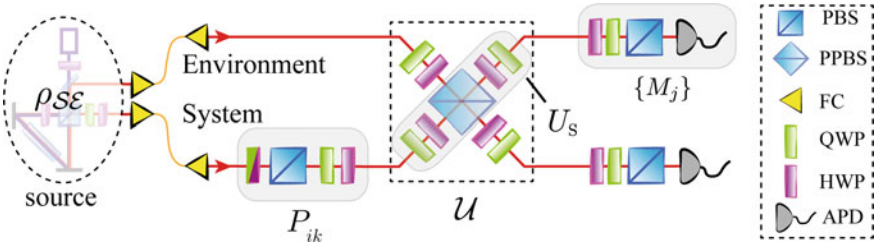

Fig. 2.5 Experimental setup. System and environment photons are created in the state ρ_{SE} with controllable degree of entanglement, using the source of Ref. [46]. Arbitary preparations $\mathcal{P}_{ij}$ on the system and measurements $\{M_j\}$ are implemented by means of polarizers (PBS), quarter- and half-wave plates (QWP, HWP) and single-photon detectors (APD). The joint system-environment evolution U is implemented as a CZ gate between a set of HWPs and QWPs. In the case of no initial correlations this setup implements the target system evolution U_S. The CZ gate is based on non-classical interference at a partially polarizing beam splitter (PPBS) with reflectivities of $r_H = 0$ ($r_V = 2/3$) for horizontally (vertically) polarized light [47]

$$|\psi\rangle_{SE} = \cos(2\theta)|H\rangle_S|V\rangle_E + \sin(2\theta)|V\rangle_S|H\rangle_E \,, \tag{2.19}$$

where $|H\rangle, |V\rangle$ correspond to horizontally and vertically polarized photons respectively. In this case the strength of the initial correlations (both quantum and classical) is parametrized by the tangle $\tau = \sin^2(4\theta)$ and can be tuned from uncorrelated ($\theta = 0$) to maximal correlation ($\theta = \pi/8$) [46]. Specifically, initial states with $\tau = \{0.012, 0.136, 0.423, 0.757, 0.908\}$ were generated, with an average fidelity of $F = 0.96(1)$ with the corresponding ideal state. The system was then subjected to the preparation procedure P_{ij}, which prepared it in the state ρ_j by first projecting onto the state ρ_i followed by a unitary rotation.

Using a set of informationally complete sets $\{|H\rangle, |V\rangle, |D\rangle, |A\rangle, |R\rangle, |L\rangle\}$ the superchannel Choi matrix $\Lambda_{\mathcal{M}}$ can be reconstructed using maximum likelihood estimation, as outlined in Sect. 2.3.2. In the case of vanishing initial correlations, the superchannel factorizes into the density matrix of the effective initial system state and the effective system channel $\Lambda_{\mathcal{M}} = \rho_S \otimes \Lambda_{\mathcal{E}}$ [34]. Hence, to allow for an operational interpretation of $\Lambda_{\mathcal{M}}$, it is best written using the state basis for the index corresponding to the effective initial state, and the Pauli basis for the indices corresponding to the effective channel. Figure 2.6b shows the results of maximum likelihood quantum process tomography for the case $U_S = H$, with different choices of preparation procedures that, in the presence of initial correlations, result in vastly different reconstructed channels. The superchannel $\mathcal{M}$ in Fig. 2.6a clearly illustrates the reason for this discrepancy: a term that corresponds to the identity operation and increases with the strength of initial correlations. This is exactly the simulated environment-induced failure mode of the system evolution.

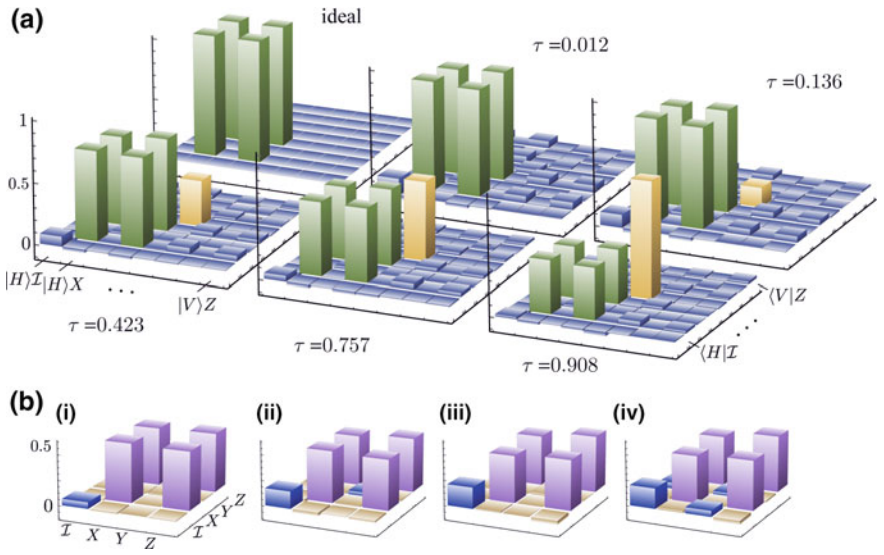

Fig. 2.6 Reconstruced superchannel Choi matrix and effective channels from quantum process tomography. **a** Real parts of $\Lambda_{\mathcal{M}}$ for $U_S = H$ in the ideal, uncorrelated case and experimental results for increasing strength of initial correlations. The matrices $\Lambda_{\mathcal{M}}$ are shown in a polarization-Pauli basis, with the elements from *left* to *right* corresponding to $\{|H\rangle, |V\rangle\} \otimes \{\mathcal{I}, X, Y, Z\}$ and from *front* to *back* corresponding to $\{\langle H|, \langle V|\} \otimes \{\mathcal{I}, X, Y, Z\}$. The emergence of a peak corresponding to the identity operation (shown in *yellow*) is characteristic for the simulated increased tendency of the single-qubit operation U_S (shown in *green*) to fail in the presence of stronger initial correlations. The negligible imaginary parts are not shown. **(b)** Real parts of the Choi-matrices (shown in the Pauli basis) for U_S obtained via quantum process tomography for different choices of preparation procedures in the case of low initial correlation $\tau = 0.136$. Cases (i) and (ii) correspond to a fixed ρ_k in Fig. 2.3b, (iii) corresponds to $\rho_k = \rho_i$, and (iv) is the case where $1 \leq k \leq 4$. The information contained in the superchannel $\mathcal{M}$ can be used to identify the optimal preparation procedure

2.3.4 *Quantifying Initial Correlations*

Initial system-environment correlations reveal themselves through their effect on the system evolution for different preparation procedures. To quantify these effects, one can define an *average initial system state* $\rho_{S,\text{av}} = \text{Tr}_{23}[\Lambda_{\mathcal{M}}]/d$ and an *average effective map* for the evolution of the system as $\Lambda_{\mathcal{E}_{\text{av}}} = \text{Tr}_1[\Lambda_{\mathcal{M}}]$. Recall that for a product initial state ($\rho_{\text{SE}} = \rho_S \otimes \rho_E$) the map $\mathcal{M}$ takes the product form $\Lambda_{\mathcal{M}} = \rho_S \otimes \Lambda_{\mathcal{E}}$. In this case $\rho_{S,\text{av}} = \rho_S$, and $\Lambda_{\mathcal{E}_{\text{av}}} = \Lambda_{\mathcal{E}}$ is the Choi matrix of the channel $\mathcal{E}$ describing the (noisy) evolution of the system alone—the same as would result from conventional quantum process tomography. For a given $\mathcal{M}$ one can now define the corresponding separable superchannel $\mathcal{M}_s$ via $\Lambda_{\mathcal{M}_s} = (\rho_{S,\text{av}} \otimes \Lambda_{\mathcal{E}_{\text{av}}})$. In general $\mathcal{M} \neq \mathcal{M}_s$ and the distance between $\mathcal{M}$ and $\mathcal{M}_s$ can be used to quantify the strength of the initial system-environment correlations. This distance is quantified by the so-called *initial correlation norm*:

$$\|\mathcal{M}\|_{\text{IC}} = \frac{1}{2}\|\mathcal{M} - \mathcal{M}_s\|_\diamond \,. \tag{2.20}$$

The matrix $\mathcal{M} - \mathcal{M}_s$ was introduced as *correlation memory matrix* in Ref. [34] since it describes how the dynamics is affected by initial correlations. The choice of the diamond norm $\|\cdot\|_\diamond$ [48] allows for an operational interpretation of the initial correlation norm in terms of channel discrimination [49]. For any two quantum channels $\mathcal{E}_1, \mathcal{E}_2$, the best single shot strategy for deciding if a given channel is $\mathcal{E}_1$ or $\mathcal{E}_2$ succeeds with probability $\frac{1}{2}\left(1 + \frac{1}{2}\|\mathcal{E}_1 - \mathcal{E}_2\|_\diamond\right)$. Thus, when $\|\mathcal{M}\|_{\text{IC}} = 0$ there is no operational difference between $\mathcal{M}$ and $\mathcal{M}_s$, which means that there are no observable system-environment correlations. This can either mean that the initial system-environment state is indeed uncorrelated, or that the environment is Markovian and initial correlations do not affect the subsequent dynamics. The initial correlation norm thus provides a necessary and sufficient condition for the decoupling of the future state of the system from its past interactions with the environment. When $\|\mathcal{M}\|_{\text{IC}} > 0$ there exists an optimal preparation procedure that can be used as a witness for initial correlations, and the specific value of the norm determines the single shot probability of success for this witness. For a more detailed discussion of the properties of this measure of initial correlation the reader is referred to Ref. [4].

Figure 2.7 shows the measured values of $\|\mathcal{M}\|_{\text{IC}}$ for the three system-environment interactions discussed in Sect. 2.3.3 for a range of simulated initial system-environment states. For all interactions, the maximum obtained value of $\|\mathcal{M}\|_{\text{IC}}$ is $\sim$0.5. This is in agreement with theoretical expectations, since for a maximally correlated initial state the simulated system-environment coupling would cause a failure of the evolution with probability 1/2.

2.3.5 *Preparation Fidelity*

The information contained in $\mathcal{M}$ can also be used to choose a set of preparation procedures that optimize the impact of the environment. Consider a system preparation via initial post-selection on the state ρ_1. The subsequent evolution is then described by the effective map

$$\Lambda_{\mathcal{E}_{\rho_1}} = \frac{1}{p_{\rho_1}} \text{Tr}_1\left[(\rho_1^\dagger \otimes \mathbb{1}_{23})\Lambda_{\mathcal{M}}\right] \,, \tag{2.21}$$

where $p_{\rho_1} = \text{Tr}\left[(\rho_1^\dagger \otimes \mathbb{1}_{23})\Lambda_{\mathcal{M}}\right]/d$ is the probability of success for the post-selection on ρ_1. Studying the effective maps in Eq. (2.21) for different ρ_1, one can optimize the preparation procedure for any desired evolution of the system. A figure of merit for this optimization is given by the *preparation fidelity* F_{prep}, which measures the fidelity between the implemented effective map $\mathcal{E}_{\rho_1}$ and the desired target channel $\mathcal{U}_S$ for initial projection onto ρ_1,

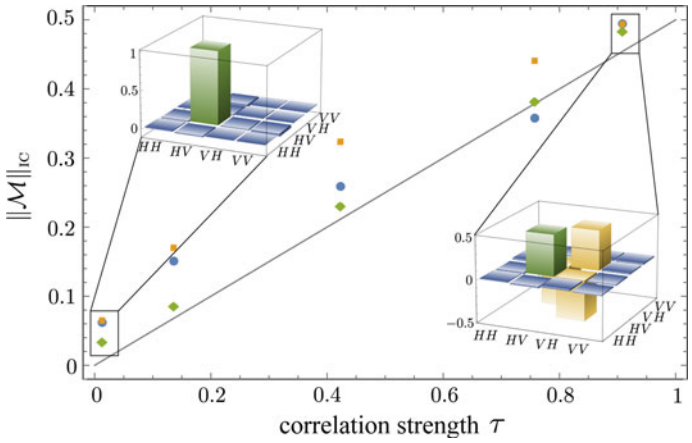

Fig. 2.7 Initial correlation norm. Shown is the initial correlation norm $\|\mathcal{M}\|_{\mathrm{IC}}$ vs the correlation strength τ of ρ_{SE} for $U = \sigma_{\mathrm{Z}}$ (blue circles), $U = H$ (yellow squares) and $U = R_{\mathrm{Y}}$ (green diamonds). The values of τ were obtained from state tomography of ρ_{SE} for each experiment. The measured real parts of the states with weakest and strongest initial correlations are shown in the respective insets. The solid line corresponds to the initial correlation norm in the ideal case. Error bars from Poissonian counting statistics are on the order of the symbol size

$$F_{\mathrm{prep}}(\mathcal{M}, \rho_1, U_{\mathrm{S}}) = \frac{1}{d^2} F(\Lambda_{\mathcal{E}_{\rho_1}}, \Lambda_{U_{\mathrm{S}}}) \,. \tag{2.22}$$

Maximizing F_{prep} over all states ρ_1 for a given target unitary U_{S} finds the preparation which comes closest to the desired U_{S}. Curiously, this is, in general, not equivalent to minimizing the impact of the environment, since the optimal preparation might harness some of the environmental correlations to improve the gate performance. Figure 2.8 a and b, show the preparation fidelity with a nominal $U_{\mathrm{S}} = Z$ and $U_{\mathrm{S}} = R_{\mathrm{Y}} Z$, respectively, calculated from an experimentally reconstructed superchannel $\mathcal{M}$ with weak initial correlations of $\|\mathcal{M}\|_{\mathrm{IC}} = 0.062(5)$ and $\|\mathcal{M}\|_{\mathrm{IC}} = 0.034(2)$, respectively. The effect of the environment is minimized for a state that is significantly different to the standard preparation $|H\rangle$, leading to an improvement in fidelity by 0.2%. This demonstrates that, even in the regime of almost uncorrelated initial system-environment states, the information contained in the superchannel can be used to improve the implemented evolution.

Alternatively, one could consider minimizing F_{prep} to find the worst-case preparation, which gives insight into where and why the experimental setup fails. Furthermore, the preparation fidelity defined in Eq. (2.22) is just one example, and one could consider other figures of merit depending on the specific scenario.

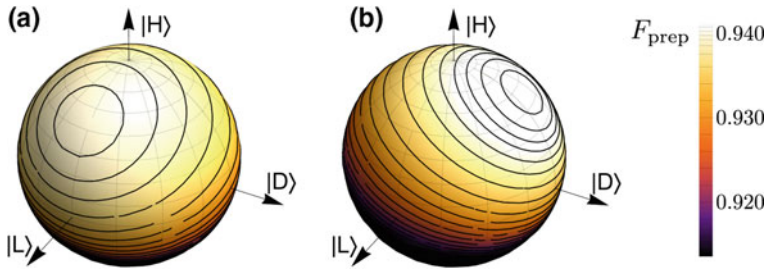

Fig. 2.8 Optimization of the preparation fidelity. The preparation fidelity $F_{\text{prep}}(\mathcal{M}, \rho_1, Z)$ for **(a)** a target $U_S = Z$ and (**b**) a target $U_S = R_Y Z$ is shown as a density plot on the surface of the Bloch sphere of the initial-projection state ρ_1. In both cases, the initial correlations are very weak, but the preparation procedure can nonetheless be used to optimize the implementation of the system evolution

2.3.6 Discussion

The superchannel approach offers an operationally motivated and experimentally accessible way of fully characterizing the reduced dynamics of a quantum system that is coupled to an environment, even in the presence of initial correlations. As a direct generalization of quantum process tomography, all the tools developed to improve the efficiency of the latter, such as compressive sensing [50, 51] can also be applied to the reconstruction of $\mathcal{M}$. Similar to process tomography, however, the reconstruction of the superchannel relies on well-characterized preparations and measurements to produce reliable estimates. In contrast to the reduced system evolution, however, the superchannel is always completely positive, and the use of maximum likelihood reconstruction is therefore justified, even in the presence of initial correlations.

On the practical side, the superchannel contains information about the initial correlations and how the environment couples to the evolution of the system. It can thus be exploited to improve the performance of the experiment, even in the regime of very weak initial correlations, as demonstrated in Sect. 2.3.5. However, since in the limit of vanishing correlations this approach essentially reduced to quantum process tomography, it is most useful in quantum architectures which are strongly coupled to their environment, such as spins in local spin baths. Another application is in quantum control, where control timescales can be much faster than environmental reset times.

On the fundamental side, the superchannel allows for the study of non-Markovian quantum processes, and the two-point correlation example here could easily be generalized to a multi-point scenario [52]. It has been suggested that such non-Markovianity could be used as a resource [53], and the superchannel approach has also been used to derive the lower bound on entropy production in a generic quantum process [54]. Interestingly, the superchannel is closely related to recent generalizations of the process matrix in the study of the causal structure of quantum

mechanics [52]. In particular, experiments such as the one presented in Sect. 2.3.3 are excellent candidates for simulating causally non-separable processes, where two operations are implemented in a superposition of causal order [55].

Acknowledgements The second part of this chapter is based on work that was first published in Ref. [18], and I have incorporated large part of the text of that paper. I would particularly like to acknowledge Christopher Wood, who was chiefly responsible for the theory developed for both, reconstruction and analysis, used in that paper, which also forms part of his PhD thesis submitted to the University of Waterloo. I have included much of this work here, as it is a vital component for the experimental application of the introduced technique. Furthermore, I would like to gratefully acknowledge Christopher Wood for introducing me to the tensor network notation and the quantum tomography methodology that I am using throughout this chapter.

References

1. Rahimi-Keshari, S., Broome, M.A., Fickler, R., Fedrizzi, A., Ralph, T.C., White, A.G.: Direct characterization of linear-optical networks. Opt. Express **21**, 13450–13458 (2013)
2. Durt, T., Englert, B.-G., Bengtsson, I., Życzkowski, K.: On mutually unbiased bases. Int. J. Quantum Inf. **8**, 535–640 (2010)
3. Renes, J.M., Blume-Kohout, R., Scott, A.J., Caves, C.M.: Symmetric informationally complete quantum measurements. J. Math. Phys. **45**, 2171–2180 (2004)
4. Wood, C. J.: Initialization and Characterization of Open Quantum Systems. Ph.D. thesis, University of Waterloo (2015)
5. Schwemmer, C., Knips, L., Richart, D., Weinfurter, H., Moroder, T., Kleinmann, M., Gühne, O.: Systematic errors in current quantum state tomography tools. Phys. Rev. Lett. **114**, 080403 (2015)
6. Shang, J., Ng, H. K., Englert, B.-G.: Quantum state tomography: Mean squared error matters, bias does not (2014). arXiv:1405.5350
7. Hradil, Z.: Quantum-state estimation. Phys. Rev. A **55**, R1561–R1564 (1997)
8. James, D.F.V., Kwiat, P.G., Munro, W.J., White, A.G.: Measurement of qubits. Phys. Rev. A **64**, 052312 (2001)
9. Blume-Kohout, R.: Optimal, reliable estimation of quantum states. New J. Phys. **12**, 043034 (2010)
10. Ferrie, C., Blume-Kohout, R.: Estimating the bias of a noisy coin. AIP Conf. Proc. **1443**, 14–21 (2012)
11. Blume-Kohout, R.: Hedged maximum likelihood quantum state estimation. Phys. Rev. Lett. **105**, 200504 (2010)
12. Home, J.P., Hanneke, D., Jost, J.D., Amini, J.M., Leibfried, D., Wineland, D.J.: Complete methods set for scalable ion trap quantum information processing. Science **325**, 1227–1230 (2009)
13. Blume-Kohout, R.: Robust error bars for quantum tomography (2012). arXiv:1202.5270
14. Knill, E., Leibfried, D., Reichle, R., Britton, J., Blakestad, R., Jost, J., Langer, C., Ozeri, R., Seidelin, S., Wineland, D.: Randomized benchmarking of quantum gates. Phys. Rev. A **77**, 012307 (2008)
15. Wallman, J.J., Flammia, S.T.: Randomized benchmarking with confidence. New J. Phys. **16**, 103032 (2014)
16. Blume-Kohout, R., Gamble, J. K., Nielsen, E., Mizrahi, J., Sterk, J. D., Maunz, P.: Robust, self-consistent, closed-form tomography of quantum logic gates on a trapped ion qubit (2013). arXiv:1310.4492
17. Blume-Kohout, R.: Private communication

18. Ringbauer, M., Wood, C.J., Modi, K., Gilchrist, A., White, A.G., Fedrizzi, A.: Characterizing quantum dynamics with initial system-environment correlations. Phys. Rev. Lett. **114**, 090402 (2015)
19. Plenio, M., Huelga, S., Beige, A., Knight, P.: Cavity-loss-induced generation of entangled atoms. Phys. Rev. A **59**, 2468–2475 (1999)
20. Bose, S., Knight, P., Plenio, M., Vedral, V.: Proposal for teleportation of an atomic state via cavity decay. Phys. Rev. Lett. **83**, 5158–5161 (1999)
21. Beige, A., Braun, D., Tregenna, B., Knight, P.L.: Quantum computing using dissipation to remain in a decoherence-free subspace. Phys. Rev. Lett. **85**, 1762–1765 (2000)
22. Diehl, S., Micheli, A., Kantian, A., Kraus, B., Büchler, H.P., Zoller, P.: Quantum states and phases in driven open quantum systems with cold atoms. Nat. Phys. **4**, 878–883 (2008)
23. Barreiro, J.T., Müller, M., Schindler, P., Nigg, D., Monz, T., Chwalla, M., Hennrich, M., Roos, C.F., Zoller, P., Blatt, R.: An open-system quantum simulator with trapped ions. Nature **470**, 486–491 (2011)
24. Cormick, C., Bermudez, A., Huelga, S.F., Plenio, M.B.: Dissipative ground-state preparation of a spin chain by a structured environment. New J. Phys. **15**, 073027 (2013)
25. Lin, Y., Gaebler, J.P., Reiter, F., Tan, T.R., Bowler, R., Sørensen, A.S., Leibfried, D., Wineland, D.J.: Dissipative production of a maximally entangled steady state of two quantum bits. Nature **504**, 415–418 (2013)
26. Xu, J.-S., Sun, K., Li, C.-F., Xu, X.-Y., Guo, G.-C., Andersson, E., Lo Franco, R., Compagno, G.: Experimental recovery of quantum correlations in absence of system-environment back-action. Nat. Comms. **4**, 2851 (2013)
27. Petruccione, F., Breuer, H.-P.: The theory of open quantum systems. Oxford University Press, Oxford (2002)
28. Modi, K., Sudarshan, E.C.G.: Role of preparation in quantum process tomography. Phys. Rev. A **81**, 052119 (2010)
29. Rodríguez-Rosario, C.A., Modi, K., Kuah, A.-M., Shaji, A., Sudarshan, E.C.G.: Completely positive maps and classical correlations. J. Phys. A **41**, 205301 (2008)
30. Modi, K.: Preparation of states in open quantum mechanics. Open. Syst. Inf. Dyn. **18**, 253–260 (2011)
31. Kuah, A.-M., Modi, K., Rodríguez-Rosario, C.A., Sudarshan, E.C.G.: How state preparation can affect a quantum experiment: Quantum process tomography for open systems. Phys. Rev. A **76**, 042113 (2007)
32. Ziman, M.: Quantum process tomography: the role of initial correlations (2006). arXiv:quant-ph/0603166
33. Carteret, H. A., Terno, D. R., Życzkowski, K.: Dynamics beyond completely positive maps: Some properties and applications. *Phys. Rev. A*, **77** (2008)
34. Modi, K.: Operational approach to open dynamics and quantifying initial correlations. Sci. Rep. **2**, 581 (2012)
35. Wißmann, S., Leggio, B., Breuer, H.-P.: Detecting initial system-environment correlations: Performance of various distance measures for quantum states. Phys. Rev. A **88**, 022108 (2013)
36. Laine, E.-M., Piilo, J., Breuer, H.-P.: Witness for initial system-environment correlations in open-system dynamics. Europhys. Lett. **92**, 60010 (2010)
37. Rodríguez-Rosario, C.A., Modi, K., Mazzola, L., Aspuru-Guzik, A.: Unification of witnessing initial system-environment correlations and witnessing non-Markovianity. Europhys. Lett. **99**, 20010 (2012)
38. Gessner, M., Breuer, H.-P.: Detecting nonclassical system-environment correlations by local operations. Phys. Rev. Lett. **107**, 180402 (2011)
39. Rossatto, D.Z., Werlang, T., Castelano, L.K., Villas-Boas, C.J., Fanchini, F.F.: Purity as a witness for initial system-environment correlations in open-system dynamics. Phys. Rev. A **84**, 042113 (2011)
40. Smirne, A., Brivio, D., Cialdi, S., Vacchini, B., Paris, M.G.A.: Experimental investigation of initial system-environment correlations via trace-distance evolution. Phys. Rev. A **84**, 032112 (2011)

41. Li, C.-F., Tang, J.-S., Li, Y.-L., Guo, G.-C.: Experimentally witnessing the initial correlation between an open quantum system and its environment. Phys. Rev. A **83**, 064102 (2011)
42. Gessner, M., Ramm, M., Pruttivarasin, T., Buchleitner, A., Breuer, H.-P., Häffner, H.: Local detection of quantum correlations with a single trapped ion. Nat. Phys. **10**, 105–109 (2013)
43. Chiuri, A., Greganti, C., Mazzola, L., Paternostro, M., Mataloni, P.: Linear optics simulation of non-markovian quantum dynamics. Phys. Rev. A **86**, 010102 (2012)
44. Schumacher, B.: Sending quantum entanglement through noisy channels. Phys. Rev. A **54**, 2614 (1996)
45. Narang, G.: Simulating a single-qubit channel using a mixed-state environment. Phys. Rev. A **75**, 032305 (2007)
46. Fedrizzi, A., Herbst, T., Poppe, A., Jennewein, T., Zeilinger, A.: A wavelength-tunable fiber-coupled source of narrowband entangled photons. Opt. Express **15**, 15377–15386 (2007)
47. Langford, N., Weinhold, T., Prevedel, R., Resch, K., Gilchrist, A.: Demonstration of a simple entangling optical gate and its use in bell-state analysis. Phys. Rev. Lett. **95**, 210504 (2005)
48. Kitaev, A.Y.: Quantum computations: Algorithms and error correction. Russ. Math. Surv. **52**, 1191 (1997)
49. Rosgen, B., Watrous, J.: On the hardness of distinguishing mixed-state quantum computations. In: 20th Annual IEEE Conference on Computational Complexity (CCC 2005), 344–354. IEEE (2005)
50. Shabani, A., Kosut, R.L., Mohseni, M., Rabitz, H., Broome, M.A., Almeida, M.P., Fedrizzi, A., White, A.G.: Efficient measurement of quantum dynamics via compressive sensing. Phys. Rev. Lett. **106**, 100401 (2011)
51. Flammia, S.T., Gross, D., Liu, Y.-K., Eisert, J.: Quantum tomography via compressed sensing: Error bounds, sample complexity, and efficient estimators. New J. Phys. **14**, 095022 (2012)
52. Pollock, F. A., Rodríguez-Rosario, C., Frauenheim, T., Paternostro, M., Modi, K.: Complete framework for efficient characterisation of non-Markovian processes (2015). arXiv:1512.00589
53. Bylicka, B., Chruscinski, D., Maniscalco, S.: Non-markovianity as a resource for quantum technologies (2013). arXiv:1301.2585
54. Vinjanampathy, S., Modi, K.: Entropy bounds for quantum processes with initial correlations. Phys. Rev. A **92**, 052310 (2015)
55. Oreshkov, O., Costa, F., Brukner, C.: Quantum correlations with no causal order. Nat. Commun. **3**, 1092 (2012)

http://www.springer.com/978-3-319-64987-0

Exploring Quantum Foundations with Single Photons

Ringbauer, M.

2017, XVIII, 208 p. 68 illus., 52 illus. in color., Hardcover
ISBN: 978-3-319-64987-0